Oxolinic Acid Binding at Goethite and Akaganeite Surfaces: Experimental Study and Modeling

Remi Marsac, Sébastien Martin, Jean-François Boily, Khalil Hanna

Article

Oxolinic Acid Binding at Goethite and Akaganéite Surfaces: Experimental Study and Modeling

Rémi Marsac, Sebastien MARTIN, Jean-François Boily, and Khalil Hanna

Environ. Sci. Technol., **Just Accepted Manuscript** • DOI: 10.1021/acs.est.5b04940 • Publication Date (Web): 17 Dec 2015

Oxolinic Acid Binding at Goethite and Akaganéite Surfaces: Experimental Study and Modeling

Rémi Marsac[1], Sébastien Martin[1,2], Jean-François Boily[2], Khalil Hanna[1*]

[1]Ecole Nationale Supérieure de Chimie de Rennes, UMR CNRS 6226, 11 Allée de Beaulieu, F-35708 Rennes Cedex 7, France.

[2]Department of Chemistry, Umeå University, Umeå, SE-901 87, Sweden.

* Corresponding author: Ecole Nationale Supérieure de Chimie de Rennes, 11 Allée de Beaulieu, F-35708 Rennes Cedex 7, France.

khalil.hanna@ensc-rennes.fr

Phone: +33 2 23 23 80 27 / Fax: +33 2 23 23 81 20

Revised manuscript to *Environmental Science and Technology*

December, 2015

Abstract

Oxolinic acid (OA) is a widely used quinolone antibiotic in aquaculture. In this study, its interactions with synthetic goethite (α-FeOOH) and akaganéite (β-FeOOH) particle surfaces were monitored to understand the potential fate of OA in marine sediments where these phases occur. Batch sorption experiments, liquid chromatography (LC) analyses of supernatants, Attenuated Total Reflectance-Fourier Transform InfraRed (ATR-FTIR) spectroscopy and multi-site complexation (MUSIC) modeling were used to monitor OA binding at these particle surfaces. Both LC and ATR-FTIR showed that adsorption did not degrade OA, and that OA adsorption was largely unaffected by NaCl concentrations (10-1000 mM). This was explained further by ATR-FTIR suggesting the formation of metal-bonded complexes at circumneutral to low pHc (= - log $[H^+]$) and with a strongly hydrogen-bonded complex at high pHc. The stronger OA binding to akaganéite can be explained both by the higher isoelectric point/point-of-zero charge (9.6-10) of this mineral than of goethite (9.1-9.4), and an additional OA surface complexation mechanism at the (010) plane. Geminal sites ($\equiv Fe(OH_2)_2^+$) at this plane could be especially reactive for metal-bonded complexes, as they facilitate a mononuclear six-membered chelate complex via the displacement of two hydroxo/aquo groups at the equatorial plane of a single Fe octahedron. Collectively, these findings revealed that Fe-oxyhydroxides may strongly contribute to the fate and transport of OA-type antibacterial agents in marine sediments and waters.

1. Introduction

Oxolinic Acid (OA) belongs to a family of quinolone antibiotics that is commonly used in aquaculture as a prophylactic, or as a chemotherapy agent.[1,2] Unabsorbed or excreted OA released into waters and/or accumulated in marine and freshwater sediments poses potential risks to public health and to aquatic life.[3] Due to its frequent use in fish farming, concentrations of OA can be of the order of 0.01–2.50 ppm in fresh or saline surface waters, 0.01–2.31 ppm in bottom waters, and even 1.81–426.31 ppm in pond sediments.[1,4,5] Moreover, Greek fish farms release 50 kg of OA annually to the Mediterranean Sea.[4]

In marine or freshwater sediments, soils and aquatic environments, the transport and mobility of quinolone antibiotics are strongly related to reactive oxide minerals through adsorption and redox reactions.[6-14] In a study on oxolinic acid sorption on marine sediments Pouliquen and Le Bris[15] concluded that while OA was not transformed in the sediments by abiotic or biotic processes, it can be sorbed to sediments containing reactive mineral surfaces. Among these reactive surfaces, iron oxyhydroxides, including goethite (α-FeOOH) and akaganéite (β-FeOOH), are ubiquitous in marine environments.[16,17] Akaganéite is a chlorine-bearing iron oxyhydroxide with a hollandite-type (tunnel-like) structure containing Cl^- ions residing in 4 × 4 nm wide tunnels running along the length of acicular nano-sized particles. This phase can be generally found in environments rich in Fe(II) and Cl^-, and as a natural corrosion product in high salinity environmental settings.[18-21] Goethite is the most thermodynamically stable iron oxyhydroxide mineral and is reported to form through the transformation of metastable phases such as ferrihydrite, schwertmannite and akaganéite.[22] Goethite was also shown to be the most common diagenetic iron oxyhydroxide in both marine and lake sediments.[23]

Although OA has been extensively used in industrial fish farming, and thus is frequently detected in surrounding waters or sediments, little is known about its molecular

interactions with suspended particles or mineral constituents in sediments, which is necessary to accurately assess its fate in aquatic environments. In this study, interactions of OA with goethite and akaganéite particles were studied by batch experiments, surface complexation modeling, and vibration spectroscopic investigations. Effects of pHc ($4 < -\log [H^+] < 11$), salinity (10-1000 mM NaCl) and surface loading on OA binding mechanisms were resolved, and implications for the fate of OA in marine environments were proposed.

2. Materials and methods

2.1. Chemicals

All chemicals used were of pro-analytical quality or better and were purchased from Sigma-Aldrich. An OA (purity > 99%) stock solution was prepared by dissolving 30 mg (115 μmoles) OA in 20 mL of 1 M NaOH, then diluted to 1 L with ultrapure water.

2.2. Synthesis and characterization of goethite and akaganéite particles

Goethite and akaganéite particles were synthesized as described in previous studies.[24,25] The synthesis procedure is given in detail in the supporting information (SI). The obtained particles were characterized by particle size and B.E.T. specific surface area N_2(g) adsorption measurements, chemical analysis, transmission electron microscopy (TEM) and X-ray diffraction (XRD). The B.E.T. specific surface area of the synthetic goethite and akaganéite were 95 and 239 m^2/g, respectively. Other characteristic properties of these solids are summarized in the SI.

2.3. Batch experiments and liquid chromatography analysis

Because high background electrolyte solutions can affect pH measurements,[27] the pH electrode was calibrated to measure the molarity of the proton (-log [H^+], noted pHc) using

94 solutions of known [H^+] (10^{-5}-10^{-3} M) at different [NaCl], and the results are provided in this
95 form in this study.

96 OA solubility experiments (undersaturation direction) were conducted by suspending
97 solid OA (~3-5 mg) in 10 mL of solution in 100 mM NaCl as a function of pHc. The
98 suspensions were equilibrated for 24 h, after which the supernatants were filtered (0.2 μm)
99 and OA concentrations were measured with high pressure liquid-chromatography coupled
100 with UV detection (HPLC-UV). As discussed later, OA solubility is relatively low (~10 μM)
101 at acidic pHc, in agreement with previous studies.[26]

102 An akaganéite (stock) suspension was prepared as previously reported.[25] Aliquots of
103 the original stock suspension (21 g/L, 5023 m^2/L) were used to prepare four suspensions (2.1
104 g/L, 502.3 m^2/L) in different concentrations of NaCl (10, 100, 450 or 1000 mM). These
105 suspensions were equilibrated for over 30 days to ensure complete ion exchange between bulk
106 akaganéite and solution ions, as previously explained by Kozin and Boily.[25] Goethite
107 suspensions were prepared at the chosen ionic strength just before adding OA.

108 Batch adsorption experiments were performed under conditions of varied reaction
109 time, OA concentration, pHc and ionic strength. Kinetic studies were conducted for pHc = 6,
110 [NaCl] = 100 mM, $[OA]_{tot}$ = 50 μM with an equivalent surface area of solids, i.e. 50 m^2/L of
111 goethite or akaganéite. All batch experiments were performed under an atmosphere of N_2(g)
112 to purge dissolved CO_2 from the aqueous solutions. Briefly, solutions of 1 to 100 μM OA
113 were mixed with goethite or akaganéite (50 m^2/L) at the desired concentration of NaCl (10,
114 100, 450 or 1000 mM). pHc was thereafter adjusted to the desired value by addition of 0.1 M
115 HCl solutions (the initial pHc value was about 10). In another set of experiments, adsorption
116 isotherms were collected at pHc = 6.1±0.1, for $[OA]_{tot}$ concentrations in the 1-50 μM range
117 for goethite, and the 3-100 μM range for akaganéite. All suspensions were then equilibrated
118 for 24 h and the supernatants filtered (0.2 μm) prior to soluble OA determination by HPLC-

UV. Desorption tests (pHc=11) were conducted under various experimental conditions as a means to verify the mass balance of OA in the systems under study.

Soluble OA concentrations were determined by a Waters 600 controller high performance liquid chromatography (HPLC) system equipped with an auto sampler (Waters 717 plus), a C18 column (250 mm×4.6 mm i.d., 5 μm) and a UV detector (275 nm, Waters 2489). The mobile phase was a mixture of water/acetonitrile (60:40 v/v) containing 0.1% of formic acid. The flow rate of the mobile phase was set at 1 mL/min in the isocratic mode. Finally, the complete experimental solubility and sorption datasets are provided in SI (Tables S1, S2 and S3).

2.4. ATR-FTIR spectroscopy

Attenuated total reflectance-Fourier transform infrared (ATR-FTIR) spectra were recorded between in the 780-4000 cm^{-1} region on an IS50 Nicolet spectrometer equipped with a KBr beamsplitter and a liquid Nitrogen cooled MCT (Mercury Cadmium Telluride) detector. A nine-reflection diamond ATR accessory (Durasampl*IR* ™, SensIR Technologies) was used for acquiring spectra of wet samples. The resolution of the single beam spectra was 4 cm^{-1}.

Three series of experiments were conducted with akaganéite for: (i) 5 < pH < with $[OA]_{tot}$=50 μM and [NaCl]=100 mM, (ii) 10 ≤ [NaCl] ≤ 1000 mM with $[OA]_{tot}$=50 μM and pHc=6 and (iii) 20 ≤ $[OA]_{tot}$ ≤ 50 μM with pHc=6 and [NaCl]=100 mM. For goethite, the same experiments were conducted except for pHc < 7, where $[OA]_{tot}$=20 μM because OA partially precipitated at 50 μM (see below). Prior to ATR-FTIR analysis, tubes from batch sorption experiments were centrifuged at 10,000 g for 30 min. Wet mineral pastes were directly and uniformly applied to the diamond ATR crystal then covered with a lid of a flow-through cell to prevent the evaporation of water. ATR-FTIR spectra were then recorded

144 immediately. Reference spectra include those for pure water, the filtered (0.2 μm) supernatant
145 from each batch adsorption experiment, as well as $OA_{(s)}$ in its solid form but covered with a
146 drop of water to apply it more uniformly. A reference spectrum of aqueous OA was also
147 acquired from a 10 mM OA (2.5 g/L) solution in 1 M NaOH. This solution ensured a
148 sufficiently high concentration of $OA^-_{(aq)}$ for ATR-FTIR analysis. Otherwise, OA was not
149 detected in any of the supernatants given its low solubility. All spectra are shown for the
150 fingerprint 1200−1800 cm^{-1} region only. Additional ATR-FTIR measurements of OA in D_2O
151 $OA^-_{(aq)}$, OA-goethite (pD = 7.81) and OA-akanagéite (pD = 8.51) in D_2O were also carried
152 out to resolve bands arising from moieties that are directly affected by exchange or hydrogen-
153 bonding with water. Sample preparation is detailed further in the Supporting Information (SI).
154

155 **2.5. Surface complexation modeling**

156 Predictions of sorption vs pHc were made using the multi-site complexation (MUSIC)
157 model approach.[28] The geochemical speciation code PHREEQC (version 2)[29] was used for
158 surface complexation calculations. PHREEQC includes the three plane model (TPM).
159 Charges of the adsorbates were distributed among the 0 (H^+, metal-bonded OA), 1 (hydrogen-
160 bonded OA), and 2 (Na^+, Cl^-) planes of the TPM. The TPM requires two capacitances for the
161 0- and the 1-plane, C_1 and C_2, respectively (see SI for more details). PhreePlot[30] was used to
162 estimate parameters for OA sorption to goethite and akaganéite. Using a modified Marquardt-
163 Levenberg procedure,[31] PhreePlot provides a statistical uncertainty for the estimated
164 parameters, which are reported in this study. For goethite or akaganéite, different types of
165 surface sites can exist depending on the proportion of crystal planes, which should have
166 different binding affinities. All information concerning the dominant crystal planes of
167 particles and corresponding site densities are given in the SI. Charge densities and
168 corresponding electrostatic interactions at particle termination (i.e. (021) plane of goethite and

(010) plane of akaganéite) were computed individually, as well as formation constants of all surface species are reported in Table 1. Surface complexation constants reported for OA were corrected according to Venema *et al.*[32] (see also[33]).

3. Results and Discussion

3.1. Batch experiments

Kinetic batch adsorption experiments conducted over a 7-day period showed that equilibrium was achieved within 2 h of reaction time (Figure S1). Desorption tests also showed that OA was removed only by adsorption or precipitation, and that breakdown by, for example, oxidation, did not occur under the experimental conditions of this study.

Adsorption curves for 10 μM OA solutions reacted in 50 m²/L mineral suspensions (Fig. 1a,b) revealed greater OA loadings on akaganéite than on goethite. At pHc < 6.5, only ~70% of OA sorbs onto goethite (Fig. 1a, Table S1) whereas an almost complete uptake was achieved on akaganéite at pHc=7.5 (~98%; Fig. 1b, Table S2). OA adsorption was greatest under acidic to circumneutral pH, and lowest under alkaline conditions, as typically encountered for anionic ligands. Furthermore, an insignificant effect of NaCl concentration was detected, so OA binding should predominantly occur as strong metal-bonded complexes with surface Fe sites and/or directly hydrogen-bonded complexes with surface hydroxo groups. Resistance of the latter to variations in ionic strength was notably demonstrated by Johnson *et al.*[34]. Weaker outer-sphere complexes should, on the other hand, be more affected by variations in ionic strength.[35] This observation is consistent with the adsorption of flumequine (analogous structure of OA) to goethite where the effect of ionic strength was also negligible (1 < [NaCl] < 100 mM).[14] Our explanation for the greater OA loadings achieved in akaganéite is two-fold. First, we note that while reactive site density of these two minerals under study are highly comparable (see details in SI), the point-of-zero charge of akaganéite

(9.6-10)[25] is higher than that of goethite (9.1-9.4)[24,36]. Second, geminal ≡$Fe(OH_2)_2^+$ groups of the (010) plane of akaganéite are expected to be strongly reactive sites for binding anionic species.[25,37,38] The site density of these groups is estimated at 0.18 site/nm² (i.e. 5% × 3.53 site/nm²), which may favor an additional OA removal mechanism, as will be suggested further by modeling (Fig. 1b and 1d).

In case of goethite (pHc < 7), the plateau is found higher for $[OA]_{tot}$=50 µM (~85%) than for $[OA]_{tot}$=10 µM (~70%) (Fig. 1a and 1c, Table S1), i.e. OA loading is more than 5 times larger at 50 µM than at 10 µM, which may suggest an additional removal mechanism such as surface or bulk precipitation of OA in this pHc range. The latter possibility was tested by conducting solubility experiments of OA at different pHc values (Fig. 2a, Table S3). Additionally, the OA solubility was calculated with PHREEQC using the acidity constant (K_a) value from the IUPAC stability constant database[39] and the solubility constant (K_s) fitted to our data with Phreeplot:

$$OAH_{(s)} \rightleftharpoons OAH_{(aq)} \quad ; \quad K_s = 10^{-5.06\pm0.07} \qquad (1)$$

$$OAH_{(aq)} \rightleftharpoons OA^- + H^+ \quad ; \quad K_a = 10^{-6.92} \qquad (2)$$

The experimental solubility values are in good agreement with both calculated (Fig. 2a) and literature data (e.g. 23 µM at pH = 7).[26] The equilibrium OA concentrations ($[OA]_{aq}$) in the presence of goethite or akaganéite at $[OA]_{tot}$=50 µM are also plotted in Figure 2a. In contact with akaganéite, $[OA]_{aq}$ is below the solubility limit for all pHc tested, ruling out the bulk precipitation in this experimental set. $[OA]_{aq}$ values in goethite are however closer to the solubility curve at pHc < 7.5, a result possibly explaining the larger loadings achieved at $[OA]_{tot}$=50 µM. Accordingly, $[OA]_{aq}$ values measured at low ligand loadings ($[OA]_{tot}$=10 µM) are below the OA solubility limit (Fig. 2a).

Adsorption isotherms (Fig. 2b) add further validation to solubility data where a sharp rise in OA removal with goethite occurred at pHc=6.1±0.1 and $[OA]_{aq}$ ≈ 10 µM,

corresponding to the solubility limit of OA. The OA adsorption isotherm for akaganéite does not, on the other hand, reach this solubility limit, but rather reaches a maximal loading corresponding to Q_{max}=1.14 OA/nm^2. This value was obtained by modeling OA-akaganéite data with the Langmuir adsorption isotherm:

$$[OA]_{sorbed} = Q_{max}\frac{K_L \times [OA]_{aq}}{1+K_L \times [OA]_{aq}} \quad (3)$$

with an adsorption constant of K_L = 0.53 μM^{-1} (see the fit with the Langmuir equation in Fig. S2). As this Q_{max} value is about one-third our estimated reactive site density at FeOOH surfaces (*i.e.* ~3 –OH/nm^2), OA surface complexes binding may realistically involve two or three –OH sites. The molecular-level nature of these interactions will however be addressed in greater detail in the following section.

3.2. ATR-FTIR Spectroscopic investigations

3.2.1. $OA_{(s)}$ and $OA^-_{(aq)}$ in 1 M NaOH

The ATR-FTIR spectra of solid and soluble OA (Fig. 3) were used as a basis for assigning surface-bound OA species. Owing to the low solubility of OA, band assignments in the soluble species were made from a 1 M NaOH solution (Fig. 3).

The absorption band of $OA_{(s)}$ and $OA_{(aq)}$ at 1040 cm^{-1} (see Figure S3) corresponds to the stretching modes of the ether group ($\nu_{C\text{-}O\text{-}C}$). The FTIR spectra of $OA_{(s)}$ and $OA_{(aq)}$ exhibit three bands with maximum absorbance between 1470 and 1510 cm^{-1}. These bands are assigned to C=C stretches ($\nu_{C=C,ring}$) and C-H bends ($\delta_{C\text{-}H,ring}$) in the aromatic and quinolinone rings.[40] The intense band of $OA_{(s)}$ at 1440 cm^{-1}, which disappears in the spectrum of $OA_{(aq)}$, may be attributed to perturbation of $\nu_{C=C,ring}$ or $\delta_{C\text{-}H,ring}$ due to intermolecular interaction in $OA_{(s)}$. The major difference between ATR-FTIR spectra of $OA_{(s)}$ and $OA_{(aq)}$ lies in the

disappearance of two bands at 1705 and 1302 cm^{-1} from the deprotonation of the carboxyl groups, *i.e.* disappearance of C=O and C-OH stretching modes of the carboxylic group. This deprotonation gives, in turn, rise to the 1395 and 1586 cm^{-1} bands, which are respectively assigned to symmetric ($\nu_{COO,s}$) and asymmetric ($\nu_{COO,as}$) stretching modes of the carboxylate, and where $\Delta\nu = \nu_{COO,as} - \nu_{COO,s} = 191$ cm^{-1}. These values are, moreover, consistent with previous studies on (fluoro)quinolones, ciprofloxacine (CIP) assigning $\nu_{COO,s}$ to a band at 1360-1380 cm^{-1},[6-11] and on ofloxacine (OFX) with a similar band at 1340 cm^{-1}.[12-14] Our spectrum for $OA_{(aq)}$ also showed a distinct band at 1340 cm^{-1}, but for reasons given later, it is not assigned to $\nu_{COO,s}$. The absorption band at 1635 cm^{-1} is assigned to the stretching of the quinolinone ring carbonyl group ($\nu_{C=O,carbonyl}$), in accordance with previous spectroscopic studies dedicated to (fluoro)quinolones.[6-14,41]

3.2.2. OA-goethite

Figure 3a shows the effect of pHc on the ATR-FTIR spectra of 20 µM OA (for pHc < 7) or 50 µM OA (for pHc >7) reacted with 50 m²/L goethite in 100 mM NaCl. As shown in Figure S3a, the characteristic features of both $OA_{(s)}$ and $OA_{(aq)}$ were observed for OA-goethite samples at pHc = 6.12 for $[OA]_{tot}$=50µM. Only the characteristic of $OA_{(aq)}$ appear for pHc ≈ 6 with $[OA]_{tot} \leq 30$ µM and for pH > 7 with $[OA]_{tot} = 50$ µM (Fig. 2, Fig. S3), in agreement with our batch results. Especially, the absence of band at 1705 cm^{-1} suggests the presence of deprotonated carboxylate groups.

At pHc = 5.20 and 6.39 ($[OA]_{tot}$=20µM), the band at 1395 cm^{-1} for $OA_{(aq)}$ almost completely disappears and is replaced by a band centered at 1340 cm^{-1}. This further supports the assignment of $\nu_{COO,s}$ to the band at 1395 cm^{-1} in $OA_{(aq)}$. The $\nu_{COO,as}$ band might be slightly blue-shifted (1590 cm^{-1}), which gives $\Delta\nu \approx 250$ cm^{-1}, a value suggesting that only one oxygen of the carboxylate binds to a surface Fe.[42] A blue shift of $\nu_{C=O,carbonyl}$ (1642 cm^{-1}) compared to

269 $OA_{(aq)}$ or $OA_{(s)}$, also suggests the involvement of the keto group in the surface complex. A
270 similar shift from protonated $OA_{(s)}$ to $Fe(OA)_{3(s)}$ was previously reported, where OA forms a
271 bidentate deprotonated complex with Fe^{3+} through the keto group and one carboxylate
272 oxygen.[41] The effects of NaCl concentration were also investigated for 20 μM OA and 50
273 m²/L goethite at pHc ≈ 6 (Fig. S3b). The weak ionic strength dependence on OA loadings and
274 ATR-FTIR spectra point to the predominance of OA species that are inner-spherically bound
275 to surface Fe sites (*i.e.* metal-bonded complex; MB), involving one oxygen of the carboxylate
276 and the oxygen of the keto group of OA. The involvement of both the carboxylate and keto
277 groups was proposed in previous studies dedicated to other quinolones binding to hydrous
278 ferric oxides[6], magnetite[9], hematite[11] and goethite[10,14] or observed for metal cation-OA
279 complexes in water.[41] The involvement of both the carboxylate and the phenolate of salicylate
280 and hydroxynaphthoate has also been evidenced at goethite surfaces.[43-46] We cannot directly
281 conclude from the ATR-FTIR spectra whether this complex involves one (Fig. 4a) or two
282 surface Fe atoms (Fig. 4b). Ideally, the steric constraints at the (101)/(001) as well as the
283 (210) planes (Pnma group) should promote bridging between two Fe atoms separated by 3 Å
284 from one another (Fig. 4b). Moreover, defects ought to expose additional possibilities for
285 mononuclear bidendate binding (*cf.* six-membered chelate complexation, Fig. 4a), namely at
286 equatorial edges of a Fe octahedron.[47]

287 At pHc = 7.60 and 8.13 ($[OA]_{tot}$=50μM), all bands remain unaffected compared to
288 pHc = 5.20 and 6.39 ($[OA]_{tot}$=20μM), except the band at 1340 cm^{-1}, which broadens and
289 whose full width at half maximum considerably increases with pHc. This band broadening is
290 taken as an indication of interactions of carboxylic groups with surface hydroxo groups with
291 various hydrogen-bond strengths (*cf.* inhomogeneous band broadening[48]). An ATR-FTIR
292 spectrum of OA-goethite recorded in D_2O for pD = 7.81 ($[OA]_{tot}$=50μM) reveals that the
293 1340 cm^{-1} band is the only one that is red-shifted in relation to the counterpart spectrum in

294 H_2O (Fig. S4), thus suggesting close interactions between carboxyl groups and O-D/H
295 moieties. These observations could thus point to a hydrogen-bonded (HB) complex involving
296 a direct hydrogen bond between carboxyl and keto moieties and surface (hydr)oxo groups.
297 This ionic strength independent complex thus contrasts with outer-sphere complexes
298 involving hydration waters.[34] The increased intensity of the band at 1340 cm^{-1} suggests that a
299 strong form of hydrogen bonding is favored at high pHc whereas metal-bonded complexation
300 is favored at low pHc. This interpretation is in line with, for example, phthalate or
301 hydroxynaphthoate sorption to goethite[44,46,47] where HB complexes are involved with two –
302 OH sites at the (101)/(001) planes (Fig. 4c).
303
304 *3.2.3. OA-akaganéite*
305 Figure 3b shows the effect of pHc on ATR-FTIR spectra of 50 µM OA interacting
306 with 50 m^2/L akaganéite in 100 mM NaCl. In agreement with our batch sorption results (Fig.
307 2), the characteristic features of $OA_{(s)}$ are absent and therefore spectra must be attributed to
308 the surface complexed OA only. This is further confirmed by the analysis of OA-akaganéite
309 samples at lower $[OA]_{tot}$ (down to 20 µM) at pHc ≈ 6 in 100 mM NaCl (Fig. S3c). The
310 spectra recorded at pHc = 5.24 and 6.20 are similar to those of OA-goethite when the amount
311 of precipitated OA is negligible, namely $\nu_{C=O,carbonyl}$ = 1642 cm^{-1} and $\nu_{COO,s}$ = 1330 cm^{-1}. The
312 intense band observed for $OA_{(aq)}$ at 1395 cm^{-1} disappears in the spectra recorded for OA-
313 akaganéite. The band of $\nu_{COO,as}$ (1590 cm^{-1}) is also slightly blue-shifted compared to $OA_{(aq)}$.
314 As for goethite, no significant effect of NaCl concentration on OA sorption to akaganéite can
315 be observed for pHc ≈ 6 (Fig. 1b), in accordance with the ATR-FTIR spectra (Fig. S3d).
316 Because these experimental conditions correspond to relatively high OA loadings (~0.5
317 OA/nm^2), formation of a bridging complex between two surface Fe involving one oxygen of
318 the carboxylate and the oxygen of the keto group of OA (Fig. 4b) is likely expected at the

(100)/(001) plane. In addition, the effect of OA surface coverage is investigated for $[OA]_{tot}$ down to 20 µM (i.e. 0.24 adsorbed OA molecule per nm²) at pHc ≈ 6 and 100 mM NaCl (Fig. S3c). At such loading, OA surface complexation to the (010) plane of akaganéite is expected to be the major sorption mechanism (Fig. 2b, Fig. S2). No change in the coordination mode of OA on akaganéite can be derived from our ATR-FTIR spectra when $[OA]_{tot}$ varies. We propose the formation of a MB surface complex involving one oxygen of the carboxylate and the oxygen of the keto group of OA. Because both water molecules of the $\equiv Fe(OH_2)_2^+$ groups can be released during the complexation of OA, we propose the formation of a six-membered chelate, involving only one Fe (Fig. 4a). Therefore, the proposed structure for the OA complex at the akaganéite (010) is presently based on crystallographic considerations.

At high pHc, we propose the predominance of a HB complex seen through a band at ~1350 cm^{-1}. This band is broad and overlaps with the band at 1330 cm^{-1}, especially for pHc = 8.02 and 8.66. Its disappearance in D_2O (Fig. S4) suggests that it is sensitive to the hydrogen bonding environment of OA, as in the case of goethite. As no significant ionic strength effects were observed, OA could be directly hydrogen bonded to surface (hydr)oxo groups of akaganéite (Fig. 4c, Fig. S3d).

3.3. Surface complexation modeling

According to the aforementioned crystallographic considerations and our spectroscopic investigations, MB surface complexes at the goethite (101)/(001) and (210) planes (Pnma group) are expected to be comparable to those on the (100) and (001) planes of akaganéite. OA forms a complex involving keto goup and one oxygen of the carboxylate group, and it can be expressed in the following reaction:

$$2\,H^+ + 2\,{\equiv}FeOH^{-0.5} + OA^- \rightleftharpoons (\equiv Fe)_2(OA)^{0\,(+1;0;0)} + 2\,H_2O \qquad \log K_{MB} \qquad (4)$$

where (+1;0;0) denotes the charge variations at the 0-, 1- and 2-planes ($\Delta z_0;\Delta z_1;\Delta z_2$). Only singly coordinated ($\equiv FeOH^{-0.5}$) surface sites are considered to be involved in the latter reaction given the propensity for ligand exchange of these sites. In the case of goethite, note that $\equiv FeOH^{-0.5}$ is used as a building block for different adsorption sites on the (101)/(001) and the (210) planes. Therefore, Eq. 4 does not denote the number of Fe(III) octahedra in a complex, but only the number of $\equiv FeOH^{-0.5}$ sites that may or may not be of the same Fe(III) octahedron.[47] Our results cannot resolve the number of Fe(III) bound to OA explicitly with the data on hand. In two recent MUSIC modeling studies, CIP[10] and OFX[14] were assumed to bind only to the goethite (210) plane. However, from our data, we cannot exclude that OA binds to the goethite (101)/(001) planes.

Hydrogen-bonded (HB) complexation could form by involving various types of surface sites. For the sake of simplicity, only singly $\equiv FeOH^{-0.5}$ sites are considered:[47]

$$2\,H^+ + 2\,\equiv FeOH^{-0.5} + OA^- \rightleftharpoons (\equiv FeOH_2)_2^{+\cdots}(OA)^{-\,(+2;-1;0)} \qquad \log K_{HB} \qquad (5)$$

Preliminary tests showed that $\log K_{HB}$ and $\log K_{MB}$ values did not significantly differ for goethite. Therefore, they were constrained at the same value during the fit. The same strategy was applied for akaganéite. According to preliminary tests, it appeared unnecessary to include an additional charge distribution (CD)[28] term, unlike previous studies dedicated to CIP[10] and OFX[14] that can bind to mineral surfaces under the zwitterion form.

Finally, to account for OA binding on the Fe sites of the (010) akaganéite plane, an additional reaction was used, which we here describe as a geminal hydroxo/aquo displacement reaction:

369 $H^+ + \equiv Fe(OH_2)(OH)^0 + OA^- \rightleftharpoons \equiv Fe(OA)^{0\,(0;0)} + 2\,H_2O$ $\log K_{(010)}$ (6)

370

371 In all of our modeling attempts, we neglect Cl^- surface complexation to the akaganéite (010)
372 plane highlighted in earlier work[25,37,38] as our data reveal no ionic strength dependence on OA
373 sorption. Cl^- surface complexation to the akaganéite (010) plane may be too weak to compete
374 significantly with OA under the present conditions.

375 Surface complexation reactions and parameters for OA are reported in Table 1.
376 Results of the fit with PhreePlot are shown in Figure 1 for pH-edges, and in Figure 2b for
377 sorption isotherms. Our model almost predicts [NaCl] independent OA loading (Fig. 1a,b).
378 Loading effects and additional apparent OA uptake on goethite (Fig. 1c), actually due to the
379 bulk precipitation of OA are also well-predicted. Speciation calculations show that about 50%
380 of 50 µM of OA precipitate in contact with goethite at pHc < 6.5, in agreement with
381 spectroscopic observations for samples prepared with high $[OA]_{tot}$ and pHc < 7 (Fig. S3a). In
382 addition, the fraction of hydrogen-bonded OA at the goethite (101)/(001) planes or akaganéite
383 (100)/(001) planes increases with pHc (Fig. S5), consistently with our FTIR data.
384 Discrepancies between experimental and modeling results are observed for akaganéite at high
385 loadings ($[OA]_{tot}$ > 20 µM; Fig. 1d, Fig. 2a), probably due to steric hindrance and/or
386 electrostatic effects at high ligand loadings. Nevertheless, the model accurately predicts OA
387 sorption to akaganéite at environmentally relevant concentrations, i.e. lower OA loadings
388 ($[OA]_{tot}$ < 20 µM; Fig. 1b, Fig. 2a).

389 The formation of a strong complex at the akaganéite (010) plane significantly
390 contributes to the overall uptake, even when the surface is almost saturated with OA. Geminal
391 sites ($\equiv Fe(OH_2)_2^+$) at this plane could be especially reactive for metal-bonded binding, as they
392 facilitate a mononuclear six-membered chelate complex via the displacement of two
393 hydroxo/aquo groups at the equatorial plane of a single Fe octahedron. This form of

394 interaction is generally excluded on the other dominant, yet idealized, (001)/(101)/(210)
395 planes of goethite and (100)/(001) of akaganéite where bridging metal-bonded and hydrogen-
396 bonded complexes are expected to be favored. The contribution of this complex is illustrated
397 e.g. in Figure 1d for $[OA]_{tot}$=50 µM, where $\equiv Fe(OA)^0$ represents about 20% of OA uptake.
398 The model predicts that the latter complex prevails at low loadings (Fig. 2b) and high pHc. In
399 our experimental conditions, for $[OA]_{tot}$=10 µM, [NaCl]=100 mM and pHc=8, $\equiv Fe(OA)^0$
400 accounts for ~65% of OA uptake on akaganéite (Fig. 1b).
401

402 **4. Environmental implications**

403 Our combined kinetic, liquid chromatographic and ATR-FTIR investigations showed that
404 only adsorption, and not oxidation, controls OA removal from aqueous suspensions of
405 goethite and akaganéite. We demonstrated that OA binds to goethite or akaganéite surfaces
406 through MB bidentate complex formation at circumneutral to low pH and through a strong
407 HB complex at high pH. The dominant MB complex involved direct binding between two
408 surface Fe with keto and carboxylate oxygens of OA, predominantly in a bridging-type
409 complex. This complexation mode was confirmed across a wide range of salinity (10 to 1000
410 mM NaCl) including seawater-like one (i.e. 599 mM). OA sorption to akaganéite is greater
411 than to goethite, a result that can be attributed to the higher isoelectric point of this mineral,
412 and also the formation of a strong complex at the akaganéite (010) plane. The contribution of
413 this strong binding with geminal sites ($\equiv Fe(OH_2)_2^+$) of the akaganéite (010) plane in the
414 overall sorption extent are strongly dependent on OA concentration. This sorption behavior
415 may explain the strong retention of OA observed in sediments containing iron mineral
416 surfaces,[15] but also to mobile FeOOH particles or colloids present in freshwater and marine
417 environments. This may also explain the slow transformation under dark conditions or high
418 persistence of OA in pond waters[49]. These results may therefore have strong implications for

the understanding of both colloidal and aqueous transport of antibacterial agents used in aquaculture.

Acknowledgements

This research was supported by "Région Bretagne" (Contract SAD-ReSolEau (8256)) as well as by the Swedish Research Council (2012-2976 to JFB).

Supporting Information Available

Details of the synthesis and characterization of goethite and akaganéite particles, surface complexation modeling; additional results for kinetic sorption/desorption, OA sorption isotherms and ATR-FTIR spectroscopy in H_2O or D_2O; tables with the whole experimental datasets. This information is available free of charge via the Internet at http://pubs.acs.org/.

References

1. Le, T. X.; Munekage, Y. Residues of selected antibiotics in water and mud from shrimp ponds in mangrove areas in Vietnam. *Mar. Pollut. Bull.*, **2004**, 49, 922–929.
2. Samuelsen, O.B. Pharmacokinetics of quinolones in fish: a review. *Aquaculture*, **2006**, 255, 55–75.
3. Samuelsen, O.B.; Ervik, A.; Pursell, L.; Smith, P. Single-dose pharmacokinetic study of oxolinic acid and vetoquinol, an oxolinic acid ester, in Atlantic salmon (Salmo salar) held in seawater and in vitro antibacterial activity against Aeromonas salmonicida. *Aquaculture*, **2000**, 187, 213–224.
4. Rigos, G.; Nengas, I.; Alexis, M.; Troisi, G.M. Potential drug (oxytetracycline and oxolinic acid) pollution from Mediterranean sparid fish farms. *Aquat. Toxicol.*, **2004**, 69, 281–288.
5. Tamtam, F.; Mercier, F.; Le Bot, B.; Eurin, J.; Tuc Dinh, Q.; Clement, M.; Chevreuil, M. Occurrence and fate of antibiotics in the Seine River in various hydrological conditions. *Sci. Total Environ.*, **2008**, 393, 84–95.
6. Gu, C.; Karthikeyan, K.G. Sorption of the Antimicrobial Ciprofloxacin To Aluminum and Iron Hydrous Oxides. *Environ. Sci. Technol.*, **2005**, 39 (23), 9166-9173.
7. Trivedi, P.; Vasudevan, D. Spectroscopic Investigation of Ciprofloxacin Speciation at the Goethite−Water Interface. *Environ. Sci. Technol.*, **2007**, 41 (9), 3153-3158.

8. Pei, Z.-G.; Shan, X.-Q.; Kong, J.-J.; Wen, B.; Owens, G. Coadsorption of ciprofloxacin and Cu(II) on montmorillonite and kaolinite as affected by solution pH, *Environ. Sci. Technol.*, **2010**, 44 (3), 915-920.

9. Rakshit, S.; Sarkar, D.; Elzinga, E.J.; Punamiya, P.; Datta, R. Mechanisms of ciprofloxacin removal by nano-sized magnetite. *J. Hazard. Mater.*, **2013**, 246-247, 221-226.

10. Gu, X.; Tan, Y.; Tong, F.; Gu, C. Surface complexation modeling of coadsorption of antibiotic ciprofloxacin and Cu(II) and onto goethite surfaces. *Chem. Eng. J.*, **2015**, 269, 113-120.

11. Martin, S.; Shchukarev, A.; Hanna, K.; Boily, J.-F. Kinetics and Mechanisms of Ciprofloxacin Oxidation on Hematite Surfaces. *Environ. Sci. Technol.*, **2015**, 49 (20), 12197–12205.

12. Goyne, K. W.; Chorover, J.; Kubicki, J. D.; Zimmerman, A. R.; Brantley, S. L. Sorption of the antibiotic ofloxacin to mesoporous and nonporous alumina and silica. *J. Coll. Int. Sci.*, **2005**, 283, 160−170.

13. Paul, T.; Machesky, M.; Strathmann, T. Surface Complexation of the Zwitterionic Fluoroquinolone Antibiotic Ofloxacin to Nano-Anatase TiO_2 Photocatalyst Surfaces. *Environ. Sci. Technol.*, **2012**, 46 (21), 11896-11904.

14. Paul, T.; Liu, J.; Machesky, M.L.; Strathmann, T. Adsorption of zwitterionic fluoroquinolone antibacterials to goethite: A charge distribution-multisite complexation model. *J. Coll. Int. Sci*,. **2014**, 428, 63-72.

15. Pouliquen, H.; Le Bris, H. Sorption of oxolinic acid and oxytetracycline to marine sediments. *Chemosphere*, **1996**, 33 (5), 801-815.

16. Burns, R. G.; Burns ,V. M. *Authigenic oxides. p. 875–914. In The Oceanic Lithosphere, Vol. 7, ed. Emiliani C.*, John Wiley & Sons, New York. **1981**.

17. Font, E.; Abrajevitch, A. Paleoenvironmental signature of the Deccan Phase-2 eruptions. *Frontiers in Earth Sciences*, **2014**, 2(23), 1-5.

18. Selwyn, L. S.; Sirois, P. J.; Argyropoulos, V. The corrosion of excavated archaeological iron with details on weeping and akaganéite. *Stud. Conserv.*, **1999**, 44, 217-232.

19. Gismelseed, A.; Elzain, M.; Yousif, A.; Al Rawas, A.; Al-Omari, I. A.; Widatallah, H.; Rais, A. Identification of corrosion products due to seawater and fresh water. *Hyperfine Interact.*, **2004**, 156, 487–492.

20. Remazeilles, C.; Refait, P. On the formation of beta-FeOOH (akaganéite) in chloride-containing environments. *Corros. Sci.*, **2007**, 49, 844–857.

21. Bibi, I.; Singh, B.; Silvester, E. Akaganéite (β-FeOOH) precipitation in inland acid sulfate soils of south-western New South Wales (NSW), Australia. *Geochim. Cosmochim. Acta*, **2011**, 75, 6429-6438.

22. Cornell, R. M.; Schwertmann, U. *The iron oxides : structure, properties, reactions, occurrences, and uses*; Wiley-VCH: Weinheim, **2003**.

23. van der Zee, C.; Roberts, D.; Rancourt, D. G.; Slomp, C. P. Nanogoethite is the dominant reactive oxyhydroxide phase in lake and marine sediments. *Geology*, **2003**, 31 (11), 993–996.

24. Gaboriaud, F.; Ehrhardt, J. J. Effects of different crystal faces on surface charge of colloidal goethite (α-FeOOH) particles: an experimental and modeling study. *Geochim. Cosmochim. Acta,* **2003**, 67, 967-983.

25. Kozin, P. A.; Boily J.-F. Proton Binding and Ion Exchange at the Akaganéite/Water Interface. *J. Phys. Chem. C*, **2013**, 117, 6409−6419.

26. Tolls, J. Sorption of veterinary pharmaceuticals in soils: a review. *Environ. Sci. Technol.*, **2001**, 35 (17), 3397-3406.

27. Altmaier, M.; Metz, V.; Neck, V.; Müller, R.; Fanghänel, Th. Solid-liquid equilibria of $Mg(OH)_{2(cr)}$ and $Mg_2(OH)_3Cl{\bullet}4H_2O_{(cr)}$ in the system Mg-Na-H-OH-Cl-H_2O at 25 °C. *Geochim. Cosmochim. Acta*, **2003**, 67, 3595-3601.

28. Hiemstra, T.; van Riemsdijk, W. H. A surface structural approach to ion adsorption: the charge distribution (CD) model. *J. Colloid Interf. Sci.*, **1996**, 179, 488-508.

29. Parkhurst, D. L.; Appelo, C. A. J. *User's guide to PHREEQC (Version 2) – a computer program for speciation, batch reaction, one-dimensional transport and inverse geochemical calculation*; Denver, Colorado, **1999**; p 312.

30. Kinniburgh, D. G.; Cooper, D. M. *PhreePlot: Creating graphical output with PHREEQC*. http://www.phreeplot.org. **2009**.

31. Powell, M. J. D. A method for minimizing a sum of squares of non-linear functions without calculating derivatives. *The Computer Journal*, **1965**, 7, 303-307.

32. Venema, P.; Hiemstra, T.; van Riemsdijk, W. H. Multisite Adsorption of Cadmium on Goethite. *J. Coll. Int. Sci.*, **1996**, 183, 515-527.

33. Lützenkirchen, J.; Marsac, R.; Kulik, D. A.; Payne, T. E.; Xue, Z.; Orsetti, S.; Haderlein, S. B. Treatment of multi-dentate surface complexes and diffuse layer implementation in various speciation codes. *Appl. Geochem.,* **2015**, 55, 128-137.

34. Johnson, B. B.; Sjöberg, S.; Persson, P. Surface Complexation of Mellitic Acid to Goethite: An Attenuated Total Reflection Fourier Transform Infrared Study. *Langmuir*, **2004**, 20, 823-828

35. Norén, K.; Persson, P. Adsorption of monocarboxylates at the water/goethite interface: The importance of hydrogen bonding. *Geochim. Cosmochim. Acta*, **2007**, 71, 5717-5730.

36. Boily, J.-F.; Lützenkirchen, J.; Blamès, O.; Beattie, J.; Sjöberg, S. Modeling proton binding at the goethite (α-FeOOH)–water Interface. *Colloids Surf. A,* **2001**, 179, 11–27.

37. Song X.; Boily, J.-F. Surface Hydroxyl Identity and Reactivity in Akaganéite *J. Phys. Chem. C*, **2011**, 115, 17036-17045.

38. Song X.; Boily, J.-F. Competitive ligand exchange on akaganéite surfaces enriches bulk chloride loadings. *J. Coll. Int. Sci.*, **2012**, 376, 331-333.

39. IUPAC (2001) *IUPAC Stability Constants Database. Version 5.4, IUPAC and Academic Software* (acadsoft@bcs.org.uk).

40. Neugebauer, U.; Szeghalmi, A.; Schmitt, M.; Kiefer, W.; Popp, J.; Holzgrabe, U. Vibrational spectroscopic characterization of fluoroquinolones. *Spectrochim. Acta, Part A*, **2005**, 61, 1505-1517.

535 41. Tarushi, A.; Christofis, P.; Psomas, G. Synthesis, characterization and interaction with
536 DNA of mononuclear metal complexes with oxolinic acid. *Polyhedron*, **2007**, 26, 3963-
537 3972.

538 42. Nakamoto, K. *Infrared and Raman Spectra of Inorganic and Coordination Compounds.*
539 *Part B: Applications in Coordination, Organometallic, and Biorganic Chemistry, 5th*
540 *ed.*; Wiley-Interscience: New York, **1997**.

541 43. Yost, E. C.; Tejedor-Tejedor, M. I.; Anderson, M. A. In Situ CIR-FTIR
542 Characterization of Salicylate Complexes at the Goethite/Aqueous Solution Interface.
543 *Environ. Sci. Technol.*, **1990**, 24, 822–828.

544 44. Cooper, E. M.; Vasudevan, D. Hydroxynaphthoic acid isomer sorption on goethite. *J.*
545 *Col. Int. Sci.*, **2009**, 333, 85–96.

546 45. Rusch, B.; Hanna, K.; Humbert, B. Sorption and Transport of Salicylate in a Porous
547 Heterogeneous Medium of Silica Quartz and Goethite. *Environ. Sci. Technol.*, **2010**, 44,
548 2447–2453.

549 46. Hanna, K.; Boily, J.-F. Sorption of Two Naphthoic Acids to Goethite Surface under
550 Flow through Conditions. *Environ. Sci. Technol.*, **2010**, 44, 8863–8869.

551 47. Boily, J.-F.; Persson, P.; Sjöberg, S. Benzenecarboxylate surface complexation at the
552 goethite (α-FeOOH)/water interface: II. Linking IR spectroscopic observations to
553 mechanistic surface complexation models for phthalate, trimellitate, and pyromellitate.
554 *Geochim. Cosmochim. Acta*, **2000**, 64 (20), 3453-3470.

555 48. Yates, J. T. Jr.; Madey, T. E. *Vibrational Spectroscopy of Molecules on Surfaces*.
556 Plenum Press, **1987**.

557 49. Lai, H-T.; Chien, Y-H. ; Lin, J-S. Long-term transformation of oxolinic acid in water
558 from an eel pond. *Aquaculture*, **2008**, 275 (1-4), 96-101.

559 50. Psomas, G.; Tarushi, A.; Efthimiadou, E. K.; Sanakis, Y.; Raptopoulou, C. P.; Katsaros,
560 N. Synthesis, structure and biological activity of copper(II) complexes with oxolinic
561 acid. *J. Inorg. Biochem.*, **2006**, 100, 1764-1773.

Table 1. Surface Complexation Model.

Goethite[a]	log K	Δz_0	Δz_1	Δz_2	(101) (Site/nm²)	(001) (Site/nm²)	(210) (Site/nm²)
$\equiv Fe_3O^{-0.5} + H^+ \rightleftharpoons \equiv Fe_3OH^{+0.5}$	9.1	+1	0	0	3.03	3.34	-
$\equiv Fe_3O^{-0.5} + H^+ + Cl^- \rightleftharpoons \equiv Fe_3OH_2^{+0.5\cdots}Cl^-$	8.1	+1	0	-1			
$\equiv Fe_3O^{-0.5} + Na^+ \rightleftharpoons \equiv Fe_3OH^{-0.5\cdots}Na^+$	-1	0	0	+1			
$\equiv FeOH^{-0.5} + H^+ \rightleftharpoons \equiv FeOH_2^{+0.5}$	9.1	+1	0	0	3.03	3.34	7.4
$\equiv FeOH^{-0.5} + H^+ + Cl^- \rightleftharpoons \equiv FeOH_2^{+0.5\cdots}Cl^-$	8.1	+1	0	-1			
$\equiv FeOH^{-0.5} + Na^+ \rightleftharpoons \equiv FeOH^{-0.5\cdots}Na^+$	-1	0	0	+1			
$2\ H^+ + 2 \equiv FeOH^{-0.5} + OA^- \rightleftharpoons (\equiv FeOH_2)_2^{+\cdots}(OA)^-$	20.3±0.1[c]	+2	-1	0			
$2\ H^+ + 2 \equiv FeOH^{-0.5} + OA^- \rightleftharpoons (\equiv Fe)_2(OA)^0 + 2\ H_2O$	20.3±0.1[c]	+1	0	0			
Akaganéite[b]	log K	Δz_0	Δz_1	Δz_2	(100)/(001) (Site/nm²)		(010) (Site/nm²)
$\equiv FeO^{-1.5} + H^+ \rightleftharpoons \equiv FeOH^{-0.5}$	20.0	+1	0	0	3.09		-
$\equiv FeO^{-1.5} + 2\ H^+ \rightleftharpoons \equiv FeOH_2^{+0.5}$	28.2	+2	0	0			
$\equiv FeO^{-1.5} + 2\ H^+ + Cl^- \rightleftharpoons \equiv FeOH_2^{+0.5\cdots}Cl^-$	29.2	+2	0	-1			
$\equiv FeO^{-1.5} + H^+ + Na^+ \rightleftharpoons \equiv FeOH^{-0.5\cdots}Na^+$	21.0	+1	0	+1			
$2\ H^+ + 2 \equiv FeOH^{-0.5} + OA^- \rightleftharpoons (\equiv FeOH_2)_2^{+\cdots}(OA)^-$	21.5±0.1[c]	+2	-1	0			
$2\ H^+ + 2 \equiv FeOH^{-0.5} + OA^- \rightleftharpoons (\equiv Fe)_2(OA)^0 + 2\ H_2O$	21.5±0.1[c]	+1	0	0			
$\equiv Fe_3O_I^{-0.5} + H^+ \rightleftharpoons \equiv Fe_3O_IH^{+0.5}$	11.7	+1	0	0	6.18		-
$\equiv Fe_3O_{II}^{-0.5} + H^+ \rightleftharpoons \equiv Fe_3O_{II}H^{+0.5}$	2.6	+1	0	0	3.09		-
$\equiv Fe_2O^{-1} + H^+ \rightleftharpoons \equiv Fe_2OH^0$	10.8	+1	0	0	3.09		7.06
$\equiv Fe_2O^{-1} + 2\ H^+ \rightleftharpoons \equiv Fe_2OH_2^+$	17.9	+2	0	0			
$\equiv Fe(OH_2)(OH)^0 + H^+ \rightleftharpoons \equiv Fe(OH_2)_2^+$	8.2	+1	0	0	-		3.53
$H^+ + \equiv Fe(OH_2)(OH)^0 + OA^- \rightleftharpoons \equiv Fe(OA)^0 + 2\ H_2O$	13.9±0.1	0	0	0			

[a]TPM with C_1=2.3 F/m², C_2=1.07 F/m², surface area: 95 m²/g; 63% of (101), 27% of (001) and 10% of (210). The HB surface complex is considered to form only at the (101) and (001) planes while the MB occurs at all planes.

[b]TPM with C_1=2.3 F/m², C_2=1.6 F/m², surface area: 239 m²/g; 95% of (100)/(001) and 5% of (010).

[c]Constant and uncertainty obtained with Phreeplot, corrected according to Venema et al.[32].

Figure captions

Figure 1. OA removal from solution (molecule / nm²) for $[OA]_{tot}$=10 µM on 50 m²/L goethite (a) and akaganéite (b) versus pHc (= -log $[H^+]$) at different NaCl concentrations. OA removal from solution (molecule / nm²) for $[OA]_{tot}$=50 µM on 50 m²/L goethite (c) and akaganéite (d) in 100 mM NaCl versus pH (= -log $[H^+]$). The corresponding percentage of OA removal at the plateau is also given. Lines are modeling results, where OA speciation on the solid phase is shown for [NaCl]=100 mM (legend in a/c and b/d is the same for the model). MB and HB refer to metal- and hydrogen-bonded OA, respectively.

Figure 2. (a) Experimental and calculated OA solubility in 100 mM NaCl versus pHc. The equilibrium OA concentration ($[OA]_{aq}$) in contact with goethite and akaganéite for $[OA]_{tot}$=10 and 50 µM in 100 mM NaCl are also plotted with modeling results. (b) OA-goethite and OA-akaganéite sorption isotherms at pHc=6.1±0.1 and 100 mM NaCl. The results of the models for goethite and akaganéite and OA speciation at the akaganéite surface are also shown. OA solubility limit at pHc=6.1 is shown as a vertical dashed line.

Figure 3. ATR-FTIR spectra of OA adsorbed to goethite (a) and akaganéite (b) for various pHc (-log $[H^+]$) in 100 mM NaCl for $[OA]_{tot}$=50 µM (except for goethite at pHc=5.20 and 6.39, where $[OA]_{tot}$=20 µM). ATR-FTIR spectra of dissolved OA in 1 M NaOH ($OA_{(aq)}$) and protonated OA under its solid form ($OA_{(s)}$) are shown as references.

Figure 4. Possible surface complexes of OA at goethite and akaganéite surfaces. The electronic structure of OA is proposed according to previous studies on metal-OA compounds.[41,50]

595 **Figure 1**

596

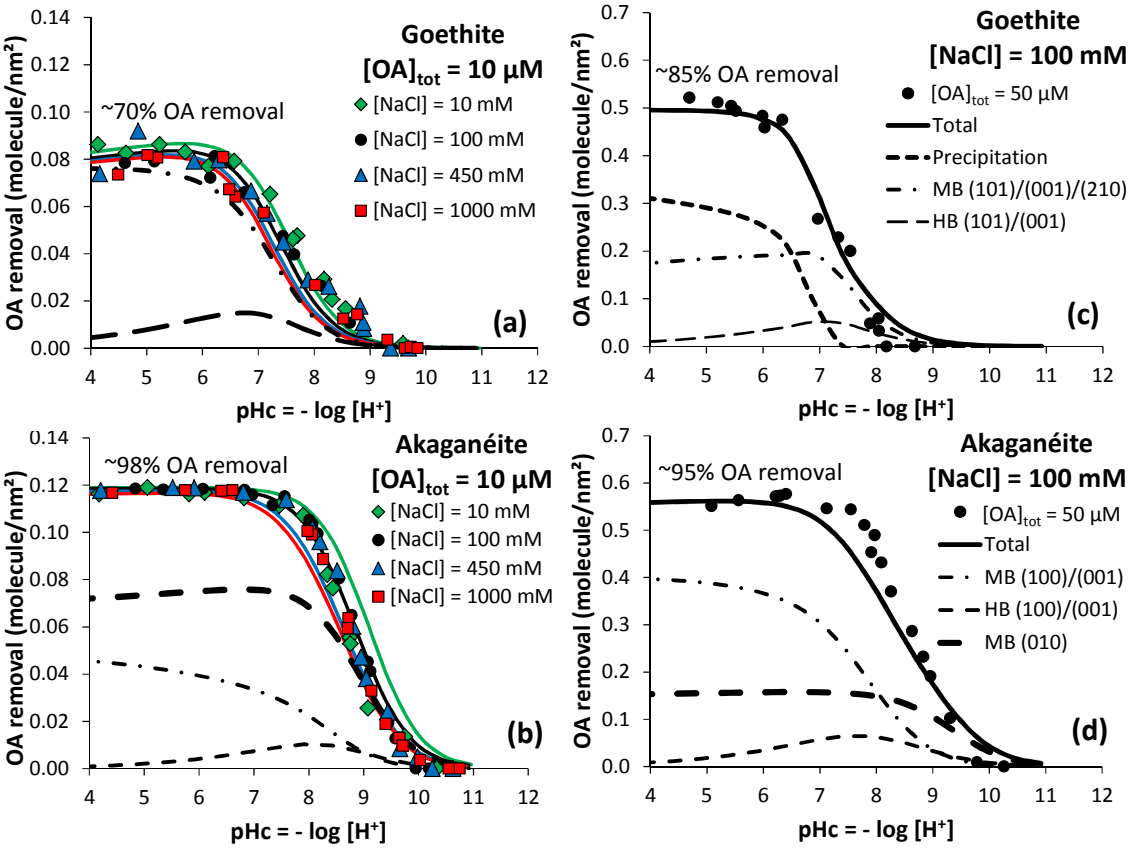

597

598

599 **Figure 2**

600

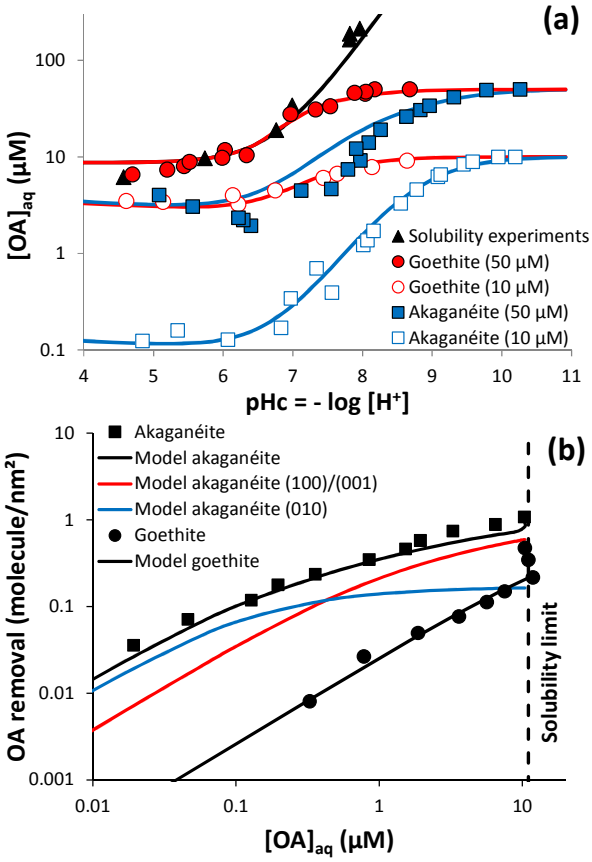

601

602

603

604 **Figure 3**

605

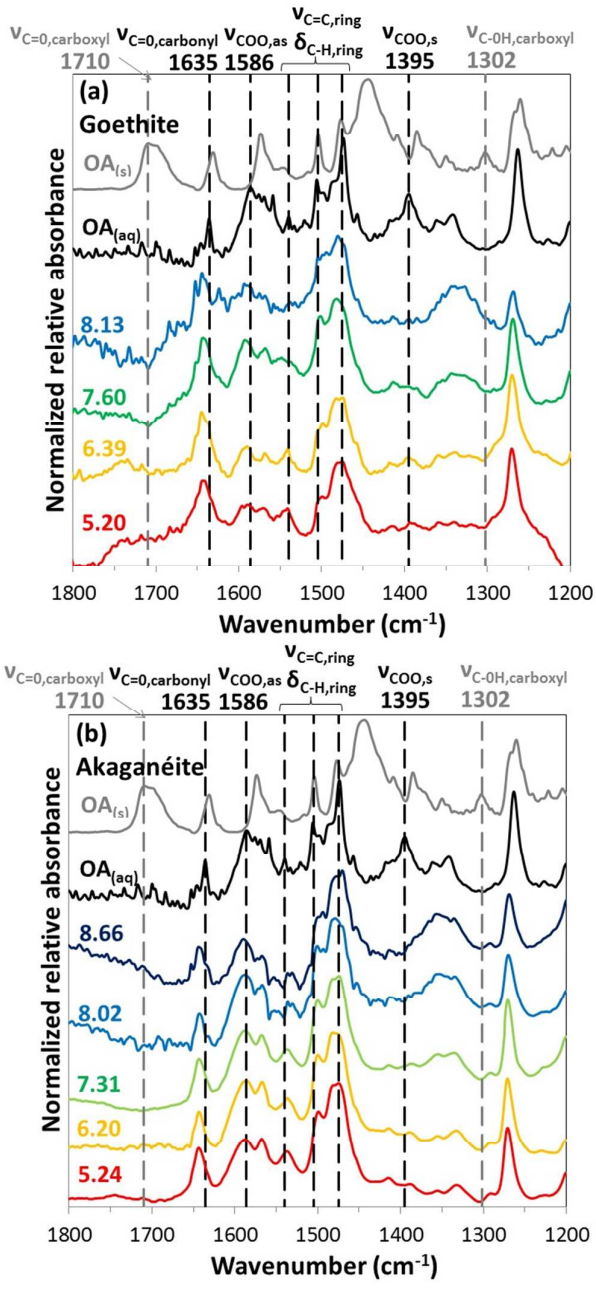

606

607 **Figure 4**

608

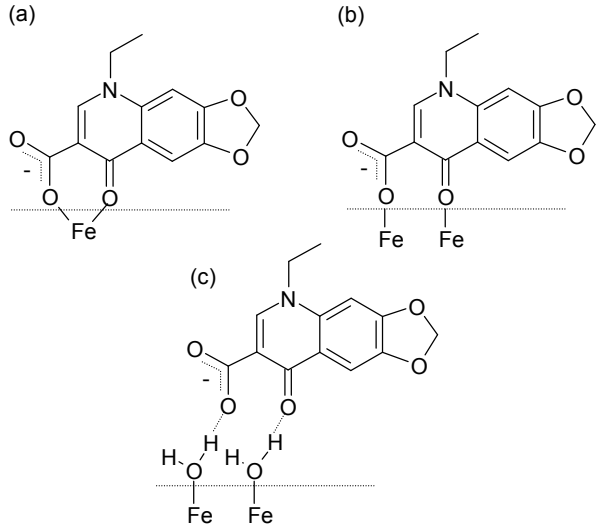

609

610

611 **TOC/abstract**

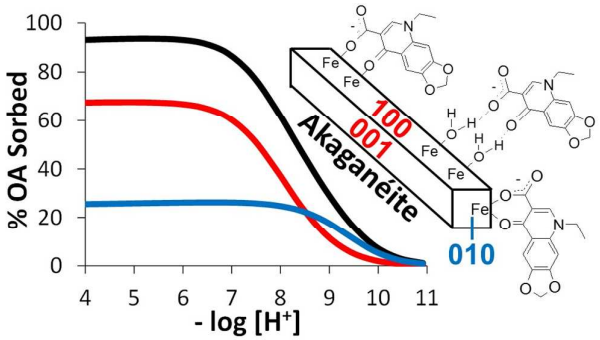

612

613